

Implementation of a Paraxial Optical Propagation Method for Large Photonic Devices

James E. Toney

Penn State University Electro-Optics Center

222 Northpointe Blvd, Freeport, PA 16229, jtoney@eoc.psu.edu

Abstract: While Comsol Multiphysics has great flexibility for modeling photonic devices, the computational demands of the general finite element method make it most suitable for small devices, on the order of a few microns in extent. Many integrated optical devices are much larger, having lengths of hundreds of microns or millimeters. A beam propagation method (BPM), which applies some simplifying assumptions that enable the use of a coarser grid or mesh, is commonly used to simulate larger devices. In this paper we present an implementation of a BPM-like method in Comsol Multiphysics and demonstrate its application to several common photonic devices.

Keywords: beam propagation method, planar lightwave circuits, integrated optics

1. Introduction

The greatest computational limitation of the finite element method for modeling electromagnetic waves is the need for a mesh that is finer than the wavelength, λ . For execution on a typical desk-top computer, this requirement limits the size of the model domain to the order of $1,000 \lambda^3$. However, if the structure is such that propagation is chiefly along a single axis (paraxial waves) the wave can be represented as an envelope function multiplied by a plane wave. The plane wave can then be factored out, and the simulation can deal only with the more slowly varying envelope function. Consequently a much coarser mesh can be used.

If the direction of propagation is taken as the z-axis, a time-harmonic, scalar wave can be represented as

$$U(\mathbf{r})=u(\mathbf{r})e^{ik_0z} \quad (1)$$

where $k_0=2\pi n_0/\lambda$, n_0 being a suitable background index – in practice the effective index of the mode being propagated. Inserting (1) into the

Helmholtz wave equation leads to the paraxial wave equation¹:

$$\nabla^2 u + 2ik_0 \partial u / \partial z + k_0^2 [(n/n_0)^2 - 1] u = 0 \quad (2)$$

where n is the local refractive index.

In most BPM methods, the next step is to assume that the envelope function is slowly varying, so that the second derivative with respect to z can be dropped to make the problem tractable in computational terms. With the Comsol FEM solvers, however, this step is entirely unnecessary. Equation (2) can be implemented via a PDE mode without further simplification.

2. Model Construction

As a test case, we have implemented a scalar, two-dimensional version of equation (2) using a PDE mode in coefficient form. The corresponding coefficients are expressed as:

$$\begin{aligned} c &= -1 \\ a &= k_0^2 ((n/n_0)^2 - 1) \\ \beta &= (0, 2 * i * k_0) \\ \text{all other coefficients} &= 0 \end{aligned} \quad (3)$$

The refractive index distribution, n , is specified via a sub-domain expression. The background index, n_0 , is defined as a constant.

2.1 Geometry, Meshing and Boundary Conditions

The geometry used consists of two, concentric, rectangular regions of space. The inner region is the active area, and the outer region is an absorbing layer to prevent reflections from the computational boundary. For the simple cases discussed here, we chose to represent the index variation by a sub-domain expression rather than having separate geometry objects for, say, the core and cladding of a waveguide.

The default meshing algorithm was used. Only the maximum sub-domain mesh size was altered. A coarser mesh was used in the absorbing layer than in the active region. Discussion of the effect of mesh size is included in Section 3.

The boundaries between the active and absorbing regions are continuity conditions, except for the input boundary on which the launch field is specified using a Dirichlet boundary condition. The outer boundary of the absorbing layer is defined to be perfectly conducting via the Dirichlet condition, $u=0$.

2.2 Absorbing Layer

An extensive formalism for perfectly matched layers has been developed for electromagnetic modeling, but here we have chosen to use a much simpler scheme. In our approach the refractive index of the absorbing layer is taken to be complex, with the real part matched to the background index of the active region and the imaginary part increasing exponentially. Thus waves can enter the absorbing layer without significant reflection but are absorbed before reaching the outer, perfectly conducting boundary. The refractive index in the absorbing region is defined as

$$n(x)=n_0 [1+ie^{\pm(x-x_0)/\Delta x}] \quad (4)$$

or an equivalent expression for the y-direction, where n_0 is the background index. x_0 and Δx are chosen so that the imaginary part is negligible at the boundary but increases rapidly enough to absorb the wave nearly entirely within the thickness of the absorbing layer.

2.3 Solving and Post-processing

The stationary solver was used with default settings in all cases. No major post-processing was performed, aside from plotting the square of the computed scalar field to represent the optical intensity.

3. Results

In this section results are presented for a few of the most common classes of optical

waveguide devices. Test cases are chosen to illustrate the ability of the method to handle the most important phenomena, including off-axis propagation and interference effects.

3.1 Straight Waveguide

The simplest case of a straight, step-index waveguide provides an illustration of how this method relaxes requirements on the mesh size. Propagation in a 100-micron long waveguide with a core index of 1.41 and a clad index of 1.40 at a wavelength of 1.5 μm is simulated with several values for the maximum mesh size, first using the paraxial mode and then using the ordinary electromagnetic propagation application mode. Figure 1 shows the results (absolute value of u) for the paraxial mode. Good results, aside from a small degree of graininess, are obtained even with a maximum element size of $3/2$ times the wavelength.

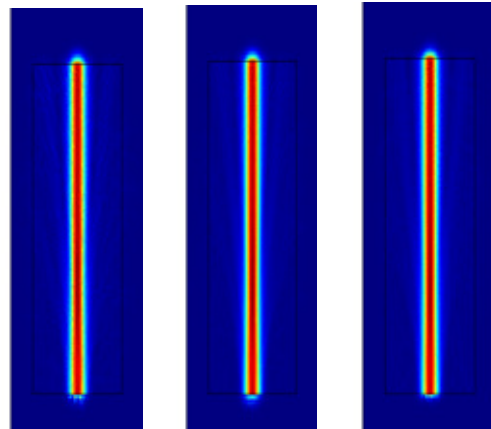


Figure 1. Simulations (absolute value of scalar field) of a 100-micron long straight waveguide with maximum mesh size = $3/2 \lambda$ (left), λ (center) and $1/2 \lambda$ (right).

Figure 2 shows results for the same waveguide geometry using the 2D, in-plane, TE-wave application mode. In this case, a maximum element size of $2\lambda/3$ produces unacceptable results, with no discernable guided-wave propagation. Even a maximum element size of $\lambda/3$ gives marginal results, with significant fluctuations in the guided wave. A maximum element size of $\lambda/6$ produces acceptable results, with only small fluctuations visible in the guided wave. Thus the paraxial method allows nearly

an order-of-magnitude increase in the coarseness of the mesh, which translates to two orders of magnitude reduction in the number of elements for a two-dimensional simulation.

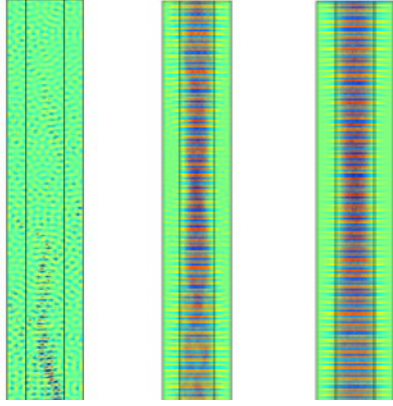


Figure 2. Simulations (z-component of electric field) of a 100-micron long straight waveguide using the 2D, in-plane TE-wave application mode with maximum mesh size = $2/3 \lambda$ (left), $1/3 \lambda$ (center) and $1/6 \lambda$ (right).

3.2 Graded-Index Waveguide

A slightly more complex example is a graded index waveguide, in which the refractive index contrast decreases with distance from the z-axis. For this case we chose a Gaussian profile of the form

$$\Delta n(x) = \Delta n_0 \exp(-x^2/\sigma^2) \quad (4)$$

The result, plotted as the square of the scalar field (intensity), for $\Delta n_0 = 0.015$ and $\sigma = 3.5 \mu\text{m}$ is shown in Figure 3. As expected for a GRIN waveguide, the wave is periodically focused.

3.3 Y-Splitter

A case that illustrates the ability of the model to handle propagation at a finite angle away from the z-axis is a y-splitter. For simplicity no attempt was made to optimize device design through the use of s-bends or tapers. Results are shown in Figure 4. Here and in subsequent examples, unless otherwise stated, the waveguide width is 4 microns, background index is 1.4, index contrast is 0.01, and wavelength is $1.5 \mu\text{m}$.

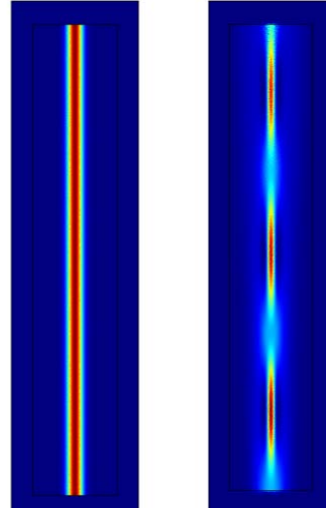


Figure 3. Simulation of 400-micron long graded-index waveguide. Refractive index distribution (left) and intensity (right).

3.4 Mach-Zehnder Interferometer

Interference effects are fully encompassed by the model, as shown by the case of a Mach-Zehnder interferometer. Results are shown in Figure 5 for two cases: zero phase difference between the two arms, leading to constructive interference at the output, and a π phase difference between the two arms, resulting in destructive interference.

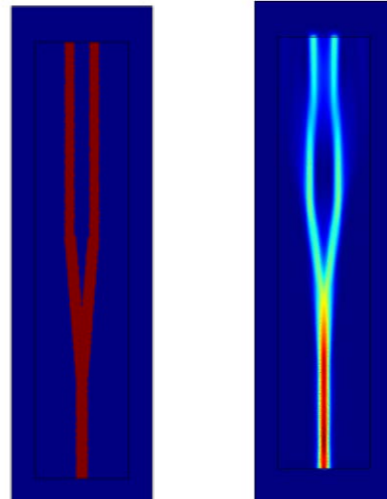


Figure 4. Refractive index distribution (left) and optical intensity (right) for 400-micron long Y-splitter.

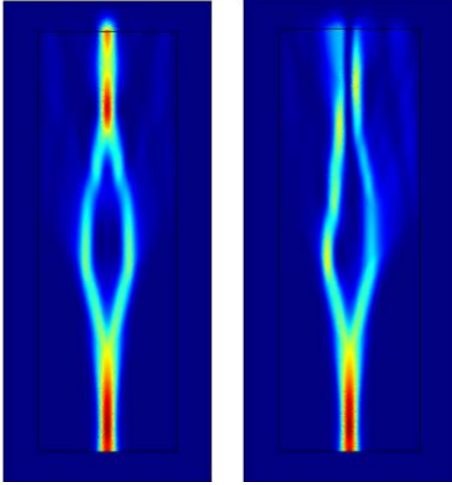


Figure 5. Simulation of 500-micron long Mach-Zehnder interferometer with no phase difference (left) and π phase difference (right) between the arms.

3.5 Directional Coupler

Another important phenomenon that is captured by the model is evanescent wave coupling between waveguides. The simplest case of a symmetrical coupler, in which the two parallel waveguides are identical, is shown in Figure 6. A wave is launched into the left waveguide and couples completely into the right waveguide over a transfer length, L . It then couples back to the left guide over an additional distance L .

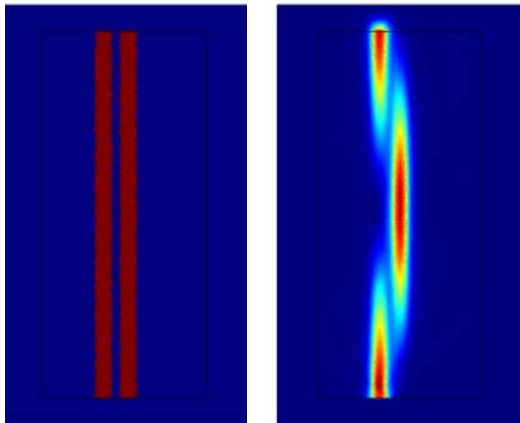


Figure 6. Refractive index distribution (left) and optical intensity (right) for a 500-micron long, symmetrical directional coupler.

The transfer length L can be calculated easily by coupled mode theory for the simple case of identical, planar waveguides². Figure 7 shows the transfer length vs. the gap between waveguides as calculated by coupled mode theory and by the paraxial model. The paraxial model gives a slightly lower value for the transfer length, especially for larger gap values. The cause of the discrepancy is not known with certainty; however it may be related to the fact that we are using a scalar model, whereas the coupled mode theory calculations were done specifically for the case of a TE mode.

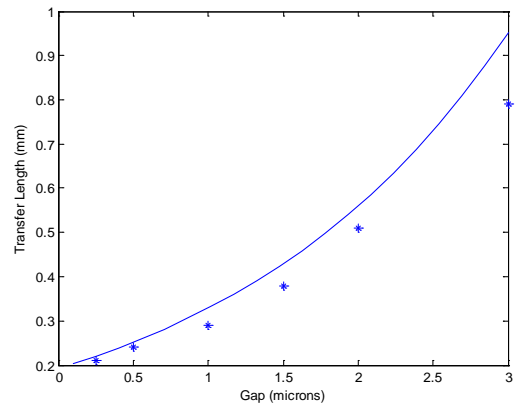


Figure 7. Transfer length as a function of gap between waveguides for a symmetrical directional coupler. Paraxial model (*) vs. coupled mode theory (line). Waveguide width=4 μm , background index=1.444, wavelength = 1.55 μm , index contrast=0.01.

3.6 Multi-mode Interference Coupler

An additional class of devices that is often simulated by BPM is multi-mode interference (MMI) couplers. An MMI device consists of one or more single-mode feeds to a multi-mode waveguide section. In our model, the input waveguide is extraneous and is omitted. Due to interference among reflections from the side walls – or equivalently beats among the modes of the multi-mode guide – multiple images of the input field are produced periodically along the length of the device. For the case in which the input field is symmetrical about the central axis of the device, the shortest length at which a two-fold image occurs is³:

$$L_2 = n_{\text{core}} W_e^2 / (2\lambda) \quad (5)$$

where W_e is the effective width of the multi-mode section, accounting for the Goos-Hanchen shift. For the parameters of our model, $L_2 \sim 400 \mu\text{m}$.

Figure 7 shows the simulation result for a 1×2 MMI splitter with $W=27 \mu\text{m}$ and $L=410 \mu\text{m}$, with a Gaussian field launched at the center of the input plane. The expected two-fold image occurs at the end of the multi-mode section and is coupled into a pair of single-mode output waveguides. This model illustrates the important fact that *glancing* reflections are accounted for by the paraxial method. It is only large-angle or backwards reflections that are beyond the scope of the paraxial approximation.

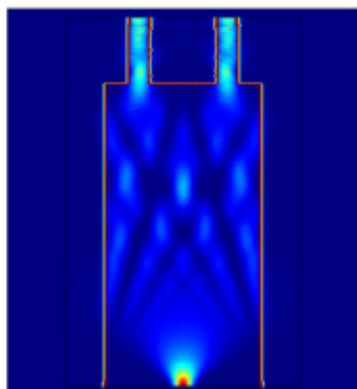


Figure 7. Intensity distribution in 1×2 MMI splitter. The multi-mode section is $410 \times 27 \mu\text{m}$. background index=1.4, $\Delta n=0.02$, $\lambda=1.55 \mu\text{m}$.

3.7 Coupling with a Microlens

An important consideration is the ability of the paraxial method to simulate high-index-contrast systems. As a test case, we modeled coupling of a free-space beam into a waveguide via a microlens, as shown in Figure 8. Here the background index is 1.0, the index of the lens and the waveguide cladding are 1.4, and the core-clad index contrast is 0.005. The waveguide width is 8 microns, and the radius of the circular lens is 100 microns. (The circular shape is not apparent in the figure due to the non-unity aspect ratio.)

In this case it was necessary to use a somewhat finer mesh ($\sim 0.45 \lambda$) to achieve adequate results. Even so, the computed field is somewhat grainy, especially in the low-intensity

areas. The result shows that the lens focuses at a distance (from the center of the lens) of approximately $200 \mu\text{m}$. For comparison, the thick lens formulation of geometrical optics⁴ predicts a focal length of $175 \mu\text{m}$.

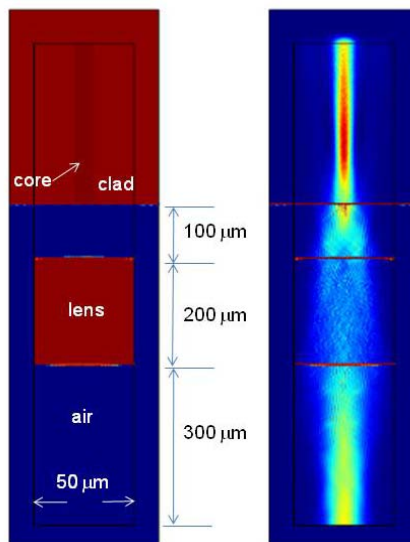


Figure 8. Refractive index distribution (left) and optical intensity for coupling of a free-space beam into a single-mode waveguide via a microlens. $n_{\text{background}}=1.0$, $n_{\text{glass}}=1.4$, $\Delta n=0.005$, $R_{\text{lens}}=100 \mu\text{m}$.

4. Extensions of the Model

All examples presented here are for the two-dimensional, scalar case. The model is directly extendable to three dimensions and non-scalar fields. Anisotropic materials can be modeled directly via the tensor nature of the coefficients. All of these enhancements increase the computational complexity and therefore reduce the advantage of the scalar approximation relative to the ordinary EM modes.

While the model discussed in this paper was implemented via a PDE mode in coefficient form, an alternative is to modify the equations in the built-in EM propagation modes of the RF/photronics module. All of the built-in features of those defined modes, including perfectly matched layers, could then be used.

5. Conclusions

Comsol Multiphysics provides a simple framework for implementation of a paraxial optical propagation mode. This method allows the use of a much coarser mesh than the ordinary electromagnetic propagation modes and thereby enables larger devices to be simulated. A two-dimensional, scalar version of this method has produced qualitatively correct simulation results for several of the most common photonic device structures, including a graded-index waveguide, y-splitter, Mach-Zehnder interferometer and directional coupler. A high-index-contrast case, coupling of a free-space beam into waveguide by a microlens, has been simulated successfully; however with practical mesh sizes the computed field in the low-intensity regions is somewhat grainy.

Combining the paraxial optical propagation mode with the multiphysics capabilities of Comsol creates the possibility of creating unified models for complex devices, such as high-speed, electro-optic modulators, thermo-optic switches and grating-based strain sensors.

6. References

1. Haus, H.A., *Waves and Fields in Optoelectronics* (Prentice Hall, Englewood Cliffs, 1984) pp. 99-100.
2. Taylor, H.F. and Yariv, A., "Guided Wave Optics," *Proc. IEEE* **62** (1974), 1044-1060.
3. Soldano, L.B. and Pennings, E.C.M., "Optical Multi-Mode Interference Devices Based on Self-Imaging: Principles and Applications," *J. Lightwave Tech.* **13** (1995), 615-627.
4. Born, M. and Wolf, E., *Principles of Optics*, 7th (expanded) ed. (Cambridge University Press, Cambridge, U.K., 1999), pp. 171-173.